Published in final edited form as:
Mol Cancer Ther. 2011 January ; 10(1): 16–28. doi:10.1158/1535-7163.MCT-10-0699.

Glutathione-Conjugate Transport by RLIP76 is required for Clathrin-Dependent Endocytosis and Chemical Carcinogenesis**

Sharad S. Singhal[1], **Dilki Wickramarachchi**[2], **Sushma Yadav**[1], **Jyotsana Singhal**[1], **Kathryn Leake**[1], **Rit Vatsyayan**[1], **Pankaj Chaudhary**[1], **Poorna Lelsani**[1], **Sumihiro Suzuki**[3], **Shaohua Yang**[4], **Yogesh C. Awasthi**[1], and **Sanjay Awasthi**[1,*]

[1] Department of Molecular Biology and Immunology, University of North Texas Health Science Center, Fort Worth, TX 76107

[3] Department of Biostatistics, School of Public Health, University of North Texas Health Science Center, Fort Worth, TX 76107

[4] Department of Pharmacology and Neuroscience, University of North Texas Health Science Center, Fort Worth, TX 76107

[2] Department of Immunology and Microbiology, The Scripps Research Institute, La Jolla, CA 92037

Abstract

Targeted depletion of the RALBP1 encoded 76 kDa splice variant, RLIP76, causes marked and sustained regression of human xenografts of lung, colon, prostate, and kidney cancer without toxicity in nude mouse models. We proposed that the remarkable efficacy and broad-spectrum of RLIP76-targeted therapy is because its glutathione-conjugate (GS-E) transport-activity is required for clathrin-dependent endocytosis (CDE), that regulates all ligand-receptor signaling, and that RLIP76 is required not only for survival of cancer cells, but also for their very existence. We studied RLIP76 mutant proteins, and the functional consequences of their expression into RLIP76$^{-/-}$ MEFs, and identified key residues for GS-E binding in RLIP76, established the requirement of RLIP76-mediated GS-E transport for CDE, and demonstrated a direct correlation between GS-E transport activities with CDE. Depletion of RLIP76 nearly completely blocked signaling down-stream of EGF in a CDE-dependent manner, and Wnt5a signaling in a CDE-independent manner. The seminal prediction of this hypothesis, that RLIP76$^{-/-}$ mice will be deficient in chemical neoplasia, was confirmed. Benzo[a]pyrene, dimethylbenzanthracene and phorbol esters are ineffective in causing neoplasia in RLIP76$^{-/-}$. PMA-induced skin carcinogenesis in RLIP76$^{+/+}$ mouse was suppressed completely by depletion of either PKCα or RLIP76 by siRNA or antisense, and could be restored by topical application of RLIP76 protein in RLIP76$^{-/-}$ mouse skin. Likewise, chemical pulmonary carcinogenesis was absent in female and nearly absent in male RLIP76$^{-/-}$ mice. In RLIP76$^{-/-}$ mice, p53, p38, and JNK activation did not occur in response to either carcinogen. Our findings demonstrate a fundamental role of RLIP76 in chemical carcinogenesis.

**This work was supported in part by USPHS grant CA 77495 and CA 104661 (SA & SS) and ES 012171 (YCA), the Cancer Research Foundation of North Texas (SS & SY) and Institute for Cancer Research & the Joe & Jessie Crump Fund for Medical Education (SS).

*Address correspondence to: Sanjay Awasthi, M.D., Professor and Associate VP for Clinical Research, University of North Texas Health Science Center, Fort Worth, TX 76107, Phone: 817-735-2654, Fax: 817-735-2118, sanjay.awasthi@unthsc.edu.

Keywords

RLIP76; drug-resistance; glutathione-conjugate transport; endocytosis

Introduction

The treatment of cancer is frequently met with disappointing outcomes due to the development of therapy-resistance in cancer cells by inappropriate activation of a number of survival-promoting proteins which include peptide hormones (ligands) such as epidermal growth factor (EGF) (1–5), transforming growth factor (TGF) (6,7), insulin-like growth factors (i.e. IGF1) and Wnt (7–10). Binding of a ligand to its specific receptor activates a number of intracellular proteins (such as Akt, RAS, NFκB) that signal the DNA to increase the expression of proteins necessary to resist apoptosis caused by stress. Receptor-ligand signaling is normally terminated after internalization of plasma membrane patches containing receptor-ligand pairs through CDE as well as caveolin-dependent endocytosis (CvDE) (1,4,11,12). Spherical membrane vesicles, which have ligand on the inner-surface and the receptor on the outer-surface, can be recycled back to the plasma membrane, or targeted for degradation, terminating signaling. However, for other ligand such as Wnt (which play a very important role in most breast cancers), CDE and CvDE appear to play opposing roles in signal activation (10,13,14). A common intersection point for signaling by EGF, TGF, IGF1 and Wnt is the activation of the potent survival protein Akt which is frequently activated in many cancers and is associated with poor survival (15).

In addition to these signaling mechanisms, the cell uses a number of small molecules to protect itself from cell death caused by toxins. Glutathione (GSH) protects cells from death caused by combining with oxidant or electrophilic toxins, both endogenous (endobiotics) and exogenous (xenobiotics), in the first committed step of the mercapturic acid pathway. Thioether glutathione-electrophile conjugates (GS-Es), formed through glutathione S-transferase (GST)-mediated catalysis, are still potentially reactive and can exert organ-specific toxicity (16–18), thus must be removed from cells using ATP-hydrolysis-dependent efflux pumps present in plasma membranes.

RLIP76 (DNP-SG ATPase), a 76 kDa splice variant encoded by human gene RALBP1 (18p11.22), is a unique and ubiquitous protein that functions in the ATP-hydrolysis dependent movement of substances at multiple sites in the cell, including plasma membrane (2,19–21), clathrin-endosomes, tubulin, chromatin, and the mitotic-spindle as an alternative splice variant known as cytocentrin (1,22–25). Knockout mouse studies show that RLIP76 provides the major catalytic-activity for the plasma membrane for efflux of GS-E from cells (1,21,26–29). RLIP76 is a stress-responsive and -protective protein that suppresses apoptosis caused by oxidant chemicals, electrophiles, and radiant energy (heat, UV, X-ray), and its stress protective function is more important for cancer cells as compared with normal cells (30–35), and the broad spectrum activity of RLIP76-targeted therapy in animal models suggests an key role in cancer.

In present studies, we have studied RLIP76 mutant proteins, and the functional consequences of their expression in RLIP76$^{-/-}$ MEFs, as well as the correlation of CDE, RLIP76 protein expression, and consequences of RLIP76-depletion. In addition, we compared the carcinogenic effects of PMA, B(a)P and DMBA in RLIP76 wild-type (RLIP76$^{+/+}$) and knockout (RLIP76$^{-/-}$) mice. Results of these studies demonstrate dramatic ablation of the carcinogenicity of these compounds in RLIP76$^{-/-}$ mice. To gain the mechanistic insight into this central role of RLIP76$^{-/-}$, we have also compared the roles of

PKCα and p53 mediated pathways and demonstrate the requirement of RLIP76 for activation of these pathways.

Methods

Reagents

Reagents were obtained from the following vendors: DOX, Adria Laboratories, Columbus, OH; ^{14}C-DOX (specific activity ~45 Ci/mmol), NEN Life Sciences, Boston, MA; [γ-^{32}P] ATP (~3000 Ci/mmol), Pharmacia Biotech, Piscataway, NJ; RLIP76-antisense (R508), Biosynthesis Inc, Lewisville, TX; RLIP76 siRNA and PKCα-siRNA, Dharmacon Research, Lafayette, CO; Phorbol 12-myristate 13-acetate (PMA, TPA, PE or phorbol ester), 7,12-dimethyl-benz[a]anthracene (DMBA), and benzo[a]pyrene (BaP), Sigma, St. Louis, MO; polyclonal rabbit-anti-human PKCα IgG, Biosource, Camarillo, CA. Apoptosis detection kit for caspase activity by ELISA, Immunochemistry Technologies; colorimetric assay for the detection of p53, total JNK, phospho-JNK, total p38 and phospho-p38, Active Motif. The source of anti-RLIP76 antibodies and DNP-SG were the same as previously described (19). RLIP76 heterozygous knockout animals (RLIP76$^{+/-}$) were generated by Lexicon genetics (The Woodlands, TX), and mice born of RLIP76$^{+/-}$ x RLIP76$^{+/-}$ mating, were genotyped by PCR strategy as described previously (26).

RLIP76 siRNA preparation

The siRNA was designed and validated as described previously (30,34). Briefly, we chose aa 171–185 (nucleotide 510–555 starting from 1 AUG codon in the open reading frame) in the N-terminal region of RLIP76 as the target region to design for siRNA because of lack of homology with other proteins or nucleotide sequences. The selected siRNA sequence was blast-search (NCBI database) against EST libraries, to ensure that only one gene is targeted. Chemically synthesized siRNA duplex in the 2′ de-protected and desalted forms, was purchased from Dharmacon Research (Lafayette, CO). The corresponding sense and antisense siRNA sequences against the targeted cDNA sequence (nt 508–528) were GAAAAAGCCAAUUCAGGAGCCdTdT and GGCUCCUGAAUUGGCUUUUUCdTdT, respectively. A 23 nucleotide long scrambled siRNA duplex was used as a control. The scrambled siRNA sequence was not homologous with RLIP76 mRNA in a blast-search against RLIP76. The sequence of the scrambled siRNA in the sense and antisense directions were GUAACUGCAACGAUUUCGAUGdTdT and CAUCGAAAUCGUUGCAGUUACdTdT, respectively. Transfection of siRNA duplexes was performed using Transmessenger Transfection Reagent kit (Qiagen) and assay for silencing 24 h after transfection. In animal studies, 200 μg (equivalent to 14 nmol) of RLIP76 siRNA was used.

RLIP76 phosphorothioate anti-sense DNA preparation (R508)

RLIP76 antisense was purchased from Biosynthesis, as described previously (31,34). The phosphorothioate antisense for RLIP76 was synthesized against the same region (nt 508–528) corresponds to RLIP76 siRNA. The oxygen in the backbone of the DNA molecules was replaced by sulfur in first and terminal three phosphate group, which makes the DNA backbone resistant to nucleases. However, the macromolecule remains electrically charged, impeding its passage across cell membrane. Selected DNA sequence was subjected to blast-search (NCBI database) against EST libraries, to ensure that only the selected gene was targeted. A 21 nucleotide long scrambled phosphorothioate DNA, which was not homologous with RLIP76 cDNA in a blast-search against RLIP76 was used as a control. The phosphorothioate DNA sequence corresponds to targeted sequence (nt 508–528) was GGCTCCTGAATTGGCTTTTTC. The sequence of the scrambled DNA was CATCGAAATCGTTGCAGTTAC. Transfection of phosphorothioate DNA was performed

using Maxfect transfection reagent (MoleculA) and assayed for silencing 24 h after transfection. In animal studies, 200 μg (equivalent to 30 nmol) of RLIP76-antisense was used.

PKCα siRNA

In this study, we used predesigned and validated chemically synthesized siRNA duplex in the 2′ de-protected and desalted forms, purchased from Dharmacon Research (Lafayette, CO) (30). A 21 nucleotide long non-silencing siRNA duplex was used as a control. The targeted cDNA sequence (GGATTGTTCTTTCTTCATA) corresponds to nt 1348–1366. The corresponding sense and antisense siRNA sequences are GGAUUGUUCUUUCUUCAUAdTdT and UAUGAAGAAAGAACAAUCCdTdT, respectively. The sequence of the non-silencing control siRNA in the sense and antisense directions are UUCUCCGAACGUGUCACGUdTdT and ACGUGACACGUUCGGAGAAdTdT, respectively. Transfection of siRNA duplexes was performed using Transmessenger Transfection Reagent kit (Qiagen) and assay for silencing 24 h after transfection. In animal studies, 200 μg (equivalent to 15 nmol) of RLIP76 siRNA was used.

Construction of substitution mutants of potential glutathione-conjugate site

Potential candidate amino acids selected through sequence alignment using IBM bioinformatics group multiple sequence alignment algorithm, were substituted with alanine using QuickChange II site directed mutagenesis kit from Stratagene, CA. Full length RLIP76 cloned to eukaryotic expression vector pcDNA 3.1 was used as the template during PCR. The genes with the confirmed mutations through DNA sequencing, were separated by digesting with restriction endonuclease BamH I and Xho I and cloned into prokaryotic expression vector pET30a(+). Regardless of the substitution mutations, all proteins were expressed to the same extent as the full length RLIP76.

Animal model for two-stage PMA carcinogenesis experiments

All animal experiments were carried out in accordance with a protocol approved by the Institutional Animal Care and Use Committee (IACUC). Eighty-eight (48 RLIP76$^{+/+}$ and 40 RLIP76$^{-/-}$) 12-weeks old mice were divided into eleven groups of 8 animals. The backs of the mice were shaved with electric clippers and the treatment was applied by a cotton applicator to a 1 cm^2 shaved area of skin on the animal's back (36,37). First of all, experimental animals were treated with 25 nmol/0.1 ml DMBA solution in acetone, to the dorsal skin, as a tumor-initiator. Treatments were as follows: **Group # 1 & 2**, RLIP76$^{+/+}$ and RLIP76$^{-/-}$ control mice (vehicle, 0.1 ml acetone treatment); **Group # 3 & 4**, RLIP76$^{+/+}$ and RLIP76$^{-/-}$ control mice (25 nmol DMBA in 0.1 ml acetone treatment); **Group # 5 & 6**, RLIP76$^{+/+}$ and RLIP76$^{-/-}$ mice treated with PMA (10 nmol PMA in 0.1 ml acetone single dose); **Group # 7 & 8**, RLIP76$^{+/+}$ and RLIP76$^{-/-}$ mice treated first with DMBA and two-weeks later followed by PMA; **Group # 9**, RLIP76$^{+/+}$ mice treated first with DMBA and two-weeks later followed by 200 μg/0.2 ml PKCα-siRNA, i.p., then PMA treatment 24 h after the PKCα siRNA treatment; **Group # 10**, RLIP76$^{+/+}$ mice treated first with DMBA and two-weeks later followed by 200 μg/0.2 ml RLIP76-antisense, i.p., then PMA treatment 24 h after the RLIP76-antisense treatment; **Group # 11**, RLIP76$^{-/-}$ mice treated first with DMBA and two-weeks later followed by 200 μg/0.2 ml RLIP76-liposomes, i.p., then PMA treatment 24 h after the RLIP76-liposomes treatment.

Effect of PMA on p53 activation in RLIP76$^{+/+}$ and RLIP76$^{-/-}$ mice tissues

Skin tissues were collected from RLIP76$^{+/+}$ and RLIP76$^{-/-}$ mice (control as well as PMA treated) after 48 h of PMA application. 10% homogenate of mouse tissues were prepared in

hypotonic buffer and nuclear extract was prepared by adding 0.5% Nonidet P-40 to the homogenate followed by centrifugation and the pellet was resuspended into the complete lysis buffer (prepared by adding 1 μL of 1 M DTT and 10 μL protease inhibitor cocktail per ml of lysis buffer, provided by the vendor) and gently shake on ice for 30 min. The supernatant (nuclear extract) was collected by centrifugation at 14, 000 × g at 4 °C and applied for assay in an Active Motif kit according to manufacturer's instructions.

Effect of PMA on total JNK, phospho-JNK, total p38 and phospho-p38 in RLIP76$^{+/+}$ and RLIP76$^{-/-}$ mice tissues

Skin tissues were collected from RLIP76$^{+/+}$ and RLIP76$^{-/-}$ mice (control and PMA treated) after 48 h of PMA application. Active Motif kits for JNK and p38 were used as per manufacturer's instruction to measure total as well as phosphorylated proteins in a 10 % homogenate prepared in complete lysis buffer (prepared by adding 1 μL of 1 M DTT and 10 μL protease inhibitor cocktail per ml of lysis buffer, provided by the vendor).

Effect of PMA on total caspase activity in RLIP76$^{+/+}$ and RLIP76$^{-/-}$ mice tissues

Skin tissues were collected from RLIP76$^{+/+}$ and RLIP76$^{-/-}$ mice (control and PMA treated) after 48 h of PMA application. Total caspase activity was determined on a 10 % homogenate was prepared in lysis buffer (10 mM Tris-HCl pH 7.4 containing 1.4 mM β-mercaptoethanol) using an Active Motif kit as per manufacturer instructions. Fluorescence was measured at excitation 550 nm and emission 595 nm, using a fluorescence plate reader (Perkin Elmer Victor 3 1420 multi-label fluorescence counter).

Animal model for B[a]P experiments

All animal experiments were carried out in accordance with a protocol approved by the Institutional Animal Care and Use Committee (IACUC). These experiments have a 2 × 2 × 2 factorial design with three independent variables (genotype, gender and drug) with 15 animals per group (total 8 groups), thus required total 120 animals for the entire study. Animals were treated with 3 mg BaP in 0.2 mL corn oil, twice 4-weeks apart (3 mg, day 1 and 29), or an equal volume of corn oil. Surviving animals were sacrificed by CO_2 inhalation followed by cervical dislocation after ~36 weeks from the beginning of the experiment and the lungs and stomach were harvested for histopathological examination. Details are provided in the figure legends.

Histological Studies

Formalin-fixed lungs and stomach from each animal were sectioned, and processed using standard histological techniques. The sections were examined using a Nikon microscope and photographed. Statistical analyses for the number of tumors between the groups were performed using Student's t-test.

Statistical Analysis

All data were evaluated with a two-tailed unpaired student's t test or compared by one-way ANOVA and are expressed as the mean ± SD. A value of $p < 0.05$ was considered statistically significant.

Results

RLIP76$^{-/-}$ MEFs are deficient in endocytosis of EGF

The linkage of RLIP76 with CDE has been demonstrated by others, showing its binding to components of CDE, though its functional significance was unknown (12,38). The binding of RLIP76 to clathrin through an adaptor protein (AP2) belonging to a family of proteins

that provide a site for binding of motor proteins in various cellular functions requiring movement, suggested that it may function as more than simply a scaffold, as previously proposed (1,39). Our studies showing that RLIP76 is an active ATPase also suggest a potential motor function of RLIP76. Though these studies indicated possible involvement of RLIP76 as an ATPase motor involved in endocytosis, it was not known whether GS-E transport was required for endocytosis. We addressed this question by identifying the GS-E conjugate binding-site of RLIP76, and designing transport deficient mutants of RLIP76 with decreased GS-E binding and transport-activity. We used the RLIP76$^{-/-}$ MEFs as a model system for testing the functional consequences of mutations. These cells lack RLIP76 entirely (Fig 1A–D). Whereas pre-immune IgG fraction recognized no epitopes on mouse MEFs, rabbit-anti-human purifed IgG fraction recognized RLIP76 only in the RLIP76$^{+/+}$ MEFs. Endocytosis of EGF-rhodamine was markedly deficient in RLIP76$^{-/-}$ cells (Fig 1E–F). The fluorescence was distributed throughout the inside of RLIP76$^{+/+}$ cells, whereas it was localized near the plasma membrane in RLIP76$^{-/-}$. This deficit of RLIP76$^{-/-}$ cells was restored almost entirely by transfecting these cells with wild-type full-length RLIP76 cDNA (Fig. 1G–H). These findings were confirmed by transfection of RLIP76$^{-/-}$ cells with GFP-RLIP76 (Fig. 1, I–P). Expression of empty GFP-vector caused no entry of the red-fluorescence of EGF-rhodamine, but GFP-RLIP76 restored this activity. These results demonstrate a requirement of RLIP76 in CDE and are consistent with our previous studies (29).

A predicted GS-E binding site in RLIP76

Potential binding site for the GSH-moiety of GS-E were predicted through sequence comparisons with GSTs and crystallins, proteins with well-defined GSH-binding motifs (40). Included in this analysis was also a less well known protein SMC-1 (structural maintenance of chromosomes), a nuclear protein that has homology with ABC-transporter proteins and is found to be up-regulated in RLIP76$^{-/-}$ mice. Alignments of RLIP76, SMC1, GSTs and crystallins were performed with the goal of determining whether the same or chemically similar amino-acid residues identified as important in GSTs and crystallin were present in RLIP76 and SMC1. Sequence alignment of crystallins with GSTs indicated the presence of 13/16 conserved GSH-binding residues of GSTs to be present in squid S-crystallin, despite the overall lack of sequence homology between GST and S-crystallin; GSTσ bears more similarity to crystallin (42–44 %) as compared to GSTα, μ, or π (19–34 %) (41,42) (Supplemental Fig. 1).

GS-E affinity of RLIP76 mutants correlates with enzymatic-activity

Putative GS-E binding-site mutants, Y231A, S234A, K237A and K244A, Y247A were created using site-directed mutagenesis. In addition, we created a double-mutant, S234A/K237A. These mutants were cloned into prokaryotic expression vectors for purification by DNPSG-affinity as described previously and their abilities to bind to the DNPSG-affinity matrix and to transport GS-E were compared. The Y231A or Y247A mutations had a slight affect on the DNPSG-affinity. The S234, K237A or K244A each reduced DNPSG-affinity more significantly. The lowest affinity was seen with the double-mutant S234/K237A (Fig. 2A). Transport-activity of these mutants was determined by measuring ATP-dependent transport of GS-E using the model substrate ^{3}H-DNP-SG after reconstituting purified proteins in artificial-liposomes (19). Decreased affinity of binding to DNP-SG correlated with decreased transport-activity. The double-mutant S234A/K237A which showed the lowest GS-E binding-affinity also had the lowest GS-E transport-activity (Fig. 2A). The compromised GS-E transport of these mutants paralleled their DNPSG-ATPase activity, consistent with reported inter-dependence of these two activities (43). Plots of DNPSG-affinity vs. either transport or ATPase indicated that DNPSG-affinity is a key determinant of substrate-stimulated ATPase-activity as well as transport (Fig. 2B).

FRET analysis confirmed reduced GS-E affinity of the S234A/K237A double-mutant

Impaired GS-E binding of the double-mutant S234A/K237A was further confirmed by examining its binding using forster resonance energy transfer (FRET) analysis, employing monochlorobimane (MCB), which gives rise to fluorescent GS-E in cells. RLIP76$^{-/-}$ MEFs transfected with wild-type RLIP76 or the S234A/K237A mutant in GFP vector were grown on sterilized cover slips, treated with 50 μM MCB and incubated for 20 min at 37 °C. Cells were fixed with paraformaldehyde and FRET and molecular interactions in cells were analyzed using time-resolved confocal microscope MT200 (Picoquant) with pulsed diode laser excitation at 405 nm for MCB donor and at 475 nm for GFP donor. MCB alone had a relatively long fluorescence life time (~11 ns) which dropped to ~3ns in presence of wild-type RLIP76 (red histogram) indicating MCB binding to RLIP76 as expected. This major shift in MCB fluorescence life-time in the presence of wild-type RLIP76 was nearly absent in presence of the S234A/K237A double-mutant, indicating a marked decrease in MCB-SG binding affinity (Figs. 2C). These results provide direct evidence of GS-E binding to RLIP76, and show a crucial role of S234 and K237 in GS-E binding and transport.

RLIP76 mutants cannot fully restore drug-resistance and CDE in RLIP76$^{-/-}$ MEFs

The question of whether the observed transport deficiency of purified recombinant RLIP76 mutant proteins would translate into deficient restoration of drug-resistance and CDE was addressed using an MEF model in which endpoints were evaluated after transient transfection with pcDNA3.1 eukaryotic transfection vector containing full-length wild-type RLIP76 or mutant cDNA. EGF-rhodamine was chosen for measurement of endocytic-activity. Transfection with wild-type RLIP76 nearly completely reversed the drug-sensitivity as well as the defect in efflux of GS-E. Melphalan is a model alkylating agent that is known to undergo obligatory metabolism to mono- and di-glutathionyl conjugates (44) which are subject to efflux by GS-E transporters. Over-expression of such transporter, including RLIP76 has been shown to decrease total accumulation of alkylating agents including melphalan in cancer cells. Because melphalan is a clinically used alkylating agent, we chose to test the drug-resistance restoration function of RLIP76 mutants by measuring the IC_{50} of melphalan by a standard MTT assay, and the total drug-accumulation (of ^{14}C-melphalan) in cells at steady-state (30 min) was measured as an inverse surrogate of melphalan-GSE efflux.

The nearly equal transfection efficiency of the vectors was confirmed by immuno-histochemistry (IHC) for RLIP76 antigen (Fig. 2D, **top-panels**). EGF-rhodamine endocytosis was determined as described above, and representative photomicrographs selected from several hundred cells of each type are presented (Fig. 2D, **bottom-panels**). Compromised transport-activity of these mutants was further confirmed by melphalan uptake and IC_{50} studies with RLIP76$^{-/-}$ MEFs transfected separately with these mutants. Results normalized to RLIP76$^{+/+}$ cells showed that melphalan accumulation was markedly increased in RLIP76$^{-/-}$ MEFs transfected with mutants as compared to wild-type transfected RLIP76$^{-/-}$ MEFs. As expected, IC_{50} of melphalan inversely correlated with its accumulation (Fig. 3A).

Endocytosis was markedly reduced in RLIP76$^{-/-}$ MEFs as compared with RLIP76$^{+/+}$, and this deficiency was nearly completely abrogated 48 h after transient transfection with wild-type RLIP76. As compared to the wild-type RLIP76, all RLIP76 mutants were clearly less efficient in restoration of endocytosis to RLIP76$^{-/-}$ MEFs. The mutant S234A/K237A which had least DNPSG-affinity, MCB-SG affinity, DNPSG-ATPase and transport-activity, and melphalan-resistance conferring activity, was also least efficient in restoring endocytosis. EGF-rhodamine endocytosis in transfected MEFs quantified by image analysis was shown to parallel melphalan resistance (Fig. 3A). When endocytosis was plotted against

the ATPase or transport activities, a saturable sigmoid relationship was evident (Fig 3B). Since GS-E affinity is lost in parallel with GS-E transport, as well as drug-resistance and CDE activities, we conclude that GS-E transport by RLIP76 is an integral requirement of CDE.

Resistance of RLIP76$^{-/-}$ mice to chemically-induced skin cancer

The transport-activity of RLIP76 is increased approximately 2-fold upon phosphorylation by PKCα at residue T^{297}. Phosphorylation at this residue, however also confers an increased proteolytic susceptibility at R^{293}. In NSCLC cells, we found that if wild-type RLIP76 was depleted by antisense targeted around T^{297}, and site deletion mutant alone was expressed, the IC_{50} of NSCLC for doxorubicin was reduced an order of magnitude, to the level seen in SCLC cell lines (27,30,45,46). In RLIP76$^{-/-}$ MEFs, DOX-resistance mediating effect and the proliferation mediating effect of PKCα are virtually absent (27). The very broad-spectrum effect of RLIP76 depletion in a number of cancer cell types indicates that RLIP76 represents a fundamental mechanism for protection of cancer cells against apoptosis. Reasoning that these mechanisms may be necessary for the very existence of cancers, we hypothesized that RLIP76$^{-/-}$ mice would be resistant to chemical carcinogenesis because cells would undergo apoptosis rather than transformation due to the lack of RLIP76. We evaluated this prediction in a model of skin carcinogenesis for which results are shown (Fig. 4). The prediction of *in-vitro* studies was confirmed *in-vivo*, showing that PMA-mediated skin-carcinogenesis is lacking in RLIP76$^{-/-}$ mouse skin. Whereas acetone or DMBA alone caused no significant changes in skin histology at 4 days after application in either genotype, PMA alone caused significant epithelial thickening and proliferation in RLIP76$^{+/+}$ mice; this response was dramatically absent in RLIP76$^{-/-}$ mouse skin. In the two-step carcinogenesis model of sequential cutaneous application of DMBA and PMA (36,37), in the RLIP76$^{+/+}$ mice, a more intense hyperporliferative response, as well as invasion were evident. In stark contrast, visually and histologically, there was no significant effect of this 2-step carcinogenesis model on the skin of RLIP76$^{-/-}$ mice. The protection was absolute, with none of the RLIP76$^{-/-}$ mice developing hyper-proliferation or invasion, whereas all RLIP76$^{+/+}$ (n=8 per group) mice developed overt and histological evidence of squamous cell carcinoma in the manner expected for this classical, accepted model of skin carcinogenesis. Remarkably, intraperitoneal injection of PKCα-siRNA or RLIP76-antisense (200 μg *i.p.*) 24 h prior to application of PMA completely blocked the visual and histological effects PMA in mice pre-treated with DMBA 13 days prior to antisense or siRNA injection (Fig. 4). These results indicated that both, RLIP76 and PKCα were required for the carcinogenic effect of PMA. Western-blots of homogenates of skin in PKCα-siRNA or RLIP76-antisense treated animals revealed appropriate suppression of the respective protein to <10% of that in the wild-type (Fig. 5 **inset**). Painting the skin of RLIP76$^{-/-}$ mice (which have constitutive PKCα) with purified RLIP76 protein reconstituted in artificial liposomes restored the ability of DMBA/PMA to cause squamous cell carcinoma in RLIP76$^{-/-}$ mice (Fig. 4). Together, these results confirmed the requirement and interdependence of RLIP76 and PKCα for carcinogenesis in this model. Activation of p53, JNK, p38 and caspase correlated with the histological results showing that the RLIP76$^{-/-}$ mice that had no significant visible or histological lesion, also did not have any significant activation of these key markers of carcinogenesis. The results presented in Fig. 4 clearly demonstrated that as expected p53, p38, JNK, and caspase 3 were activated in carcinogen treated RLIP76$^{+/+}$ mice. Only a minimal activation of these markers was seen in RLIP76$^{-/-}$ mice and it could be restored completely by RLIP76 proteoliposomes. These results further indicated the requirement of both, PKCα and RLIP76 for PMA-induced carcinogenesis in this model.

These studies were repeated, substituting the sequential application of DMBA and PMA both in acetone with a single application of PMA dissolved in $CHCl_3$ (chloroform, a

chlorinated hydrocarbon that is also metabolized by P450 to produce mutagenic stress). Surprisingly, more dramatic results were seen in this model with very clear and extensive invasion as well as inflammatory changes evident in the skin of RLIP76$^{+/+}$ mice at day 4. Again, in stark contrast with RLIP76$^{+/+}$ mice, no hyperproliferative response or invasion were seen in the skin of RLIP76$^{-/-}$ mice. As with the DMBA/PMA model, p53, JNK, p38 and caspase activation was minimal/lacking in RLIP76$^{-/-}$ mice as compared to that with RLIP76$^{+/+}$ mice. Blockade of gross, histological, and signaling effects by PKCα-siRNA or RLIP76-antisense was also evident in the chloroform/PMA skin carcinogenesis model (Fig. 5). The Western-blot analyses of skin tissues showed expected absence of RLIP76 in RLIP76$^{-/-}$ mouse skin, successful depletion of skin RLIP76 or PKCα by the antisense or siRNA treatment (Fig. 5, **inset**). Application of RLIP76-proteoliposomes to skin of RLIP76$^{-/-}$ mice to restore the carcinogenic and signaling effects of chloroform/PMA concurred with observations with the DMBA/PMA model (Fig. 4).

Reduction of BaP-induced lung carcinogenesis in RLIP76$^{-/-}$ mice

To determine whether resistance to chemical-carcinogenesis of RLIP76$^{-/-}$ mice was a phenomenon particular to the skin, we performed studies with another well established model. B[a]P administered by gavage that is known to cause multiple pulmonary adenocarcinomas with a high frequency (>50%) and gastric adenocarcinomas with a somewhat lower frequency (20–30%). We have previously shown gender-specific differences in susceptibility to B[a]P-induced carcinogenesis (47). In present studies, we used our previously established conditions to compare chemically-induced lung and fore-stomach neoplasia in RLIP76$^{+/+}$ and RLIP76$^{-/-}$ mice after oral exposure to B[a]P. No death occurred and no cancers were found in either stomach or lung in the vehicle treated control animals (Fig 6A). All RLIP76$^{+/+}$ animals that became moribund and died during the course of experiments, or were euthanized (5 males, 7 females) were from the B[a]P treated groups, and all had either pulmonary or gastric adenocarcinomas or both. Neither of the two RLIP76$^{-/-}$ males that died during the course of experiments had detectable malignancy at autopsy. The incidence of pulmonary adenocarcinomas and gastric adenocarcinomas at the end of the study (including autopsy findings in animals with early death) were determined. The results of these studies showed that as compared with vehicle controls, incidence of malignancy among all B[a]P treated RLIP76$^{+/+}$ animals was 26/30, whereas among all RLIP76$^{-/-}$ animals treated with B[a]P] incidence of malignancy was only 2/30. The lowest incidence of malignancy was in RLIP76$^{-/-}$ females (1/15), and the highest in RLIP76$^{+/+}$ males (14/15) (Fig. 6B).

In general, females were found to be less susceptible to B[a]P carcinogenesis as compared with males. Representative histological sections from animals from each group are also presented (Fig. 6C). As with DMBA/PMA or chloroform/PMA, activation of p53, JNK, p38 and caspase were measured in lung and stomach tissues. P53 was significantly activated (over 3 fold) in male, and to a lesser extent (2 fold) in the female RLIP76$^{+/+}$ animals. P38 was less remarkably activated in the male lung, and nearly unchanged in the female. JNK was also less affected than p53 in both male and female. Caspase3 was activated in both genders to the same extent. Activation of all these markers in stomach tissue was less marked in both male and female RLIP76$^{+/+}$ mice. Activation of the all four signaling proteins was significantly, but not completely suppressed in the lungs as well as stomachs of all RLIP76$^{-/-}$ mice (Fig. 6D & E). These results demonstrate that the RLIP76$^{-/-}$ mice are also highly resistant to BaP induced neoplasia, and strengthen the argument for a fundamental role of RLIP76 in carcinogenesis, and the fundamental need of RLIP76 for cancer.

Discussion

Results of present studies demonstrate for the first time that GS-E transport by RLIP76 is an integral requirement for CDE. These findings fundamentally alter the view of the mechanism of CDE and the mechanisms that function to provide energy for this process. They show that the ATP-dependent efflux of glutathionylated-metabolites generated from the oxidative metabolism of polyunsaturated fatty acids is the rate determining step of CDE. Thus, cellular oxidative stress levels functions, as sensed by the mercapturic acid pathway, serve as an over-arching control of receptor-ligand signaling. Thus, diseases as varied as cancer, diabetes, inflammatory bowel disease, neurodegenerative disorders, and others, in which oxidative stress plays a promoting and initiating role, the present model predicts that the responsiveness of diseased cells to ligand-mediated signaling will be reduced, as a consequence of oxidative stress, only if RLIP76 is present. The veracity of this assertion is amply demonstrated by the fact that despite markedly elevated levels of oxidative-stress in the form of lipid-hydroperoxides and reactive lipid-derived aldehydes and alkenals (26,28) (up to 7 fold higher in some tissues) and suppressed GSH-linked antioxidant enzyme activities, the RLIP76$^{-/-}$ animals are resistant to both cancer, and diabetes (48). The resistance to carcinogenesis is more significant considering that signaling pathways including JNK, Akt, PI3K, and ERK1/2 known to be activated in cancer as well as diabetes are activated in the tissues and MEFs of RLIP76$^{-/-}$ mice at baseline, and not further affected by carcinogens (28). Remarkably, the same animals are highly sensitive to the acute toxicity of chemicals (including carcinogens) and to radiation poisoning (26,28,29). The degree of resistance of RLIP76$^{-/-}$ mouse to two different carcinogens is also quite remarkable, that would place RLIP76 among the most potent oncogene, and strongly indicate an existential role of RLIP76 in cancer; that is, inappropriately increased RLIP76 is necessary for triggering the subsequent steps of carcinogenesis. Because exogenous electrophilic compounds (xenobiotics) are effluxed as native species as well as GSH-conjugates through this mechanism, there exists a great potential for drug-interactions as well as therapeutic effects. Because the binding partners of RLIP76 (HSF1, POB1) are known to be involved in regulating stress responses, and insulin-responses (respectively), selectively targeting these inter-protein interactions could yield high value drugs for prevention and treatment of these diseases linked with excessive lipid peroxidation (22,48).

Lipid peroxidation is a common chemical reaction triggered by both chemical and radiant carcinogens, and acute high dose exposure to these carcinogenic insults to normal cells is known to induce expression as well and altered sub-cellular distribution of RLIP76 that is known to control the master heat-shock transcription factor Hsf-1 that regulates expression of damage-repair and chaperone proteins (22). In normal cells, an increase in 4-HNE levels is accompanied with a transient increase in cellular RLIP76 that functions to restore 4-HNE levels to baseline (22,49). Because 4-HNE is itself known to trigger a variety of signaling including proliferation, differentiation, and apoptosis in a concentration dependent manner, the function of RLIP76 would be construed as opposing 4HNE mediated signaling (49). Cancer cells have constitutively elevated RLIP76 protein levels; this is despite very low 4-HNE levels characteristic of cancer cells (31), suggesting that the normal regulatory mechanisms for suppressing RLIP76 under conditions of low 4-HNE does not function properly. Because a variety of receptor-ligand signaling also generates lipid-peroxidation and at very low concentrations 4-HNE is known to cause proliferation, it is not unreasonable to speculate that perception of these low-amplitude signals would be enhanced in a low 4-HNE environment typical of cancer cells (49).

Among the most common therapies of cancer, X-irradiation and anthracycline are known to induce lipid-peroxidation, and result in increased production of 4-HNE and GS-HNE. Alkylating agents and platinum coordinates are known to be metabolized to GS-E, which are

competitive substrate inhibitors of GS-HNE efflux. Vinca alkaloids as well are known to be direct competitive substrate inhibitors of RLIP76-mediated transport, and their efficacy in lung cancer xenografts is markedly enhanced by RLIP76 blockade by antibody or depletion by antisense or siRNA constructs (32). Thus, a majority of all cancers are already being treated with approaches that result in functional inhibition of a physiological function of RLIP76 that maintains low levels of 4-HNE through ATP-dependent efflux of GS-HNE.

PMA is believed to function primarily through activation of PKCα (27), though PKC-independent mechanisms have been suggested (50). In RLIP76$^{-/-}$ mice, complete lack of hyper-proliferative response to PMA indicates that both mechanisms are non-functional in the absence of RLIP76. The inflammatory response, also down-stream of PKCα through NFkB, remained intact in the RLIP76$^{-/-}$ mice indicated by skin edema and slight erythema and a minimal inflammatory infiltrate in the dermis. The lack of PKCα-proliferative effects shown previously in RLIP76$^{-/-}$ MEFs is validated by present *in-vivo* findings, and strongly indicates the phosphorylation of RLIP76 by PKCα is a necessary pre-requisite for the hyperproliferative response to PMA (27,30). The lack of PMA-mediated activation of p53 in wild-type mice treated with PKCα siRNA confirms that p53 activation is down-stream of PKCα; the lack of PKCα-mediated hyper-proliferative response in RLIP76$^{-/-}$ mice and in RLIP76$^{+/+}$ mice depleted of RLIP76 by antisense, places RLIP76 down-stream of PKCα functionally. This finding confirms the results of previous studies showing that PKCα activates GS-E transport and ATPase-activities of RLIP76 through phosphorylation of RLIP76 at multiple sites, principally T^{297} and S^{353} (45). This idea is also entirely consistent with the well established role of PKCα in regulating CDE.

A hallmark of exposure to mutagens (chemical and radiant) is the activation of p53, and consequent cell-cycle arrest through interactions with p21. The mechanisms of p53 activation include JNK, p38, other stress-kinases that can be activated down-stream of PKCα. There is no evidence that RLIP76 interacts directly with p53. Indirect interaction of RLIP76 and p53 appears possible because Hsf-1, the heat-shock master-transcription factor, binds both RLIP76 and p53. The Hsf1-p53 complex is known to translocate to the nucleus in response to stress, just as the Hsf1-RLIP76 complex does (22). Whether these are competing complexes or whether there exist ternary complexes containing all three proteins is not yet known. A more conventional explanation for the lack of activation of p53 by PMA in RLIP76$^{-/-}$ would be that JNK and p38 which function to activate p53 are themselves not activated. Transfection studies in RLIP76$^{-/-}$ MEFs with dominant negative and constitutively active mutants of JNK, as well as AKT and ERK1/2, have shown that the stress-protective effect of these proteins is considerably blunted in the absence of RLIP76 (28).

Summary

Our previous studies have characterized and established the role of RLIP76 in enhancing proliferative potential and multi-drug resistance of cancer cells. RLIP76 is over-expressed in many cancers as characterized by our previous studies (31–35). RLIP76 inhibition is selectively toxic to tumor cells and does not affect the normal cells both *in vivo* and *in vitro*. Our present studies advance the oncogenic role of RLIP76 by systematically characterizing the existential requirement of RLIP76 for carcinogen induced oncogenic transformation of normal cells. Our findings directly validate the crucial role of up-regulated mercapturic acid pathway early in carcinogenesis, and concur with abundant pathological and clinical evidence for a central role of this pathway in the phenotype of multi-drug resistance. Present studies provide compelling evidence for an integral rate-limiting role of GS-E transport by RLIP76 in CDE, and provide the signaling framework for understanding the global and cancer-specific growth inhibitory and pro-apoptotic effects of RLIP76 inhibition. RLIP76 represents a unique target in cancer therapy because it functions not only as the rate

regulatory step in mercapturic acid pathway but also significantly determines endocytosis. The former is crucial for protection of cells from stressors including oxidation, chemical toxins, and radiation. The latter impact on endocytosis serves as a master regulator of receptor-ligand signaling. In addition, we demonstrate the complete lack of DMBA-PMA skin carcinogenesis, and near complete lack of BaP-carcinogenesis, accompanied by failure to activate key cancer-critical survival pathways in RLIP76$^{-/-}$ mice, and propose an existential role of RLIP76 in carcinogenesis. In summary, in addition to previously established role of RLIP76 inhibition in causing complete regression of tumors, our present observations strongly infer the mechanistic relevance and potential therapeutic benefits of targeting RLIP76 in populations predisposed to significant oncogenic chemical insults due to exposure to environmental or occupational carcinogens. These studies should help lay the foundation for further clinical studies aimed at RLI76 targeted anti-cancer therapeutics.

Supplementary Material

Refer to Web version on PubMed Central for supplementary material.

Abbreviations used are

RLIP76	Ral-interacting protein
GSH	glutathione
GS-E	glutathione-conjugates
DNP-SG	dinitrophenyl-S-glutathione
DOX	doxorubicin
4-HNE	4-hydroxynonenal
FRET	forster resonance energy transfer
MEFs	mouse embryonic fibroblasts
CDE	clathrin-dependent endocytosis

References

1. Awasthi S, Singhal SS, Sharma R, Zimniak P, Awasthi YC. Transport of glutathione-conjugates and chemotherapeutic drugs by RLIP76: a novel link between G-protein and tyrosine-kinase signaling and drug-resistance. Int J Cancer. 2003; 106:635–46. [PubMed: 12866021]
2. Awasthi S, Singhal SS, Srivastava SK, et al. Adenosine-triphosphate-dependent transport of doxorubicin, daunomyicn, and vinblastine in human tissues by a mechanism distinct from the P-glycoprotein. J Clin Invest. 1994; 93:958–65. [PubMed: 7907606]
3. Huang Y. Pharmacogenetics/genomics of membrane transporters in cancer chemotherapy. Cancer Metastasis Rev. 2007; 26:183–201. [PubMed: 17323126]
4. Yadav S, Zajac E, Singhal SS, Awasthi S. Linking stress-signaling, glutathione-metabolism, signaling pathways and xenobiotic-transporters. Cancer Metas Rev. 2007; 26:59–69.
5. Desbois-Mouthon C, Baron A, Blivet-Van Eggelpoël MJ, et al. Insulin-like growth factor-1 receptor inhibition induces a resistance mechanism via the epidermal growth factor receptor/HER3/AKT signaling pathway: rational basis for cotargeting insulin-like growth factor-1 receptor and epidermal growth factor receptor in hepatocellular carcinoma. Clin Cancer Res. 2009; 15:5445–56. [PubMed: 19706799]
6. Watabe T, Miyazone K. Roles of TGF-beta family signaling in stem cell renewal and differentiation. Cell Res. 2009; 19:103–115. [PubMed: 19114993]

7. Guo Q, Manolopoulou M, Bian Y, Schilling AB, Tang WJ. Molecular basis for the recognition and cleavages of IGF-II, TGF-alpha, and amylin by human insulin-degrading enzyme. J Mol Biol. 2010; 395:430–43. [PubMed: 19896952]
8. Baserga R, Peruzzi F, Reiss K. The IGF-1receptor in cancer biology. Int J Cancer. 2003; 107:873–7. [PubMed: 14601044]
9. Pollak M. Insulin and insulin-like growth factor signaling in neoplasia. Nat Rev Cancer. 2008; 8:915–28. [PubMed: 19029956]
10. Iozzo RV, Eichstetter L, Danielson KG. Aberrant expression of the growth factor Wnt-5a in human malignancy. Cancer Res. 1995; 55:3495–9. [PubMed: 7627953]
11. Laniosz V, Holthusen KA, Meneses PI. Bovine papillomavirus type 1: from clathrin to caveolin. J Virol. 2008; 82:6288–98. [PubMed: 18417596]
12. Matsuzaki T, Hanai S, Kishi H, Liu Z, Bao Y, Kikuchi A. Regulation of endocytosis of activin type II receptors by a novel PDZ protein through Ral/Ral-binding protein 1-dependent pathway. J Biol Chem. 2002; 277:19008–18. [PubMed: 11882656]
13. Zhang Y, Zhang B. TRAIL resistance of breast cancer cells is associated with constitutive endocytosis of death receptors 4 and 5. Mol Cancer Res. 2008; 6:1861–71. [PubMed: 19074831]
14. Pedersen NM, Madshus IH, Haslekås C, Stang E. Geldanamycin-induced down-regulation of ErbB2 from the plasma membrane is clathrin dependent but proteasomal activity independent. Mol Cancer Res. 2008; 6:491–500. [PubMed: 18337455]
15. Rini BI, Atkins MB. Resistance to targeted therapy in renal-cell carcinoma. Lancet Oncol. 2009; 10:992–1000. [PubMed: 19796751]
16. Jakoby WB. The glutathione S-transferases: a group of multi-functional detoxification protein. Adv Enzymol Mol Biol. 1978; 46:383–414.
17. Awasthi YC, Sharma R, Singhal SS. Human glutathione S-transferases. Int J Biochem. 1994; 26:295–308. [PubMed: 8187927]
18. Hayes JD, Pulford DJ. The glutathione S-transferase supergene family: regulation of GST and the contribution of the isoenzymes to cancer chemoprotection and drug resistance. Crit Rev Biochem Mol Biol. 1995; 30:445–600. [PubMed: 8770536]
19. Awasthi S, Cheng J, Singhal SS, et al. Novel function of human RLIP76: ATP-dependent transport of glutathione-conjugates and doxorubicin. Biochemistry. 2000; 39:9327–34. [PubMed: 10924126]
20. Stuckler D, Singhal J, Singhal SS, Yadav S, Awasthi YC, Awasthi S. RLIP76 transports vinorelbine and mediates drug-resistance in non-small cell lung cancer. Cancer Res. 2005; 65:991–8. [PubMed: 15705900]
21. Singhal SS, Yadav S, Roth C, Singhal J. RLIP76: A novel glutathione-conjugate and multi-drug transporter. Biochem Pharmacol. 2009; 77:761–9. [PubMed: 18983828]
22. Singhal SS, Yadav S, Drake K, Singhal J, Awasthi S. Hsf-1 and POB1 induce drug-sensitivity and apoptosis by inhibiting Ralbp1. J Biol Chem. 2008; 283:19714–29. [PubMed: 18474607]
23. Quaroni A, Paul EC. Cytocentrin is a Ral-binding protein involved in the assembly and function of the mitotic-apparatus. J Cell Sci. 1999; 112:707–18. [PubMed: 9973605]
24. Hu Y, Mivechi NF. HSF-1 interacts with Ral-binding-protein 1 in a stress-responsive, multi-protein complex with HSP90 *in vivo*. J Biol Chem. 2003; 278:17299–306. [PubMed: 12621024]
25. Vatsyayan R, Lelsani P, Awasthi S, Singhal SS. RLIP76: A versatile transporter and an emerging target for cancer therapy. Biochem Pharmacol. 2010; 79:1699–705. [PubMed: 20097178]
26. Awasthi S, Singhal SS, Yadav S, et al. RALBP1 is a major determinant of radiation sensitivity. Cancer Res. 2005; 65:6022–8. [PubMed: 16024601]
27. Singhal SS, Yadav S, Singhal J, Awasthi YC, Awasthi S. Mitogenic and drug-resistance mediating effects of PKCα require RLIP76. Biochem Biophys Res Commun. 2006; 348:722–7. [PubMed: 16890208]
28. Singhal J, Singhal SS, Yadav S, et al. RLIP76 in defense of radiation poisoning. Int J Rad Oncol Biol Phys. 2008; 72:553–61.

29. Singhal SS, Yadav S, Singhal J, Sahu M, Sehrawat A, Awasthi S. Diminished drug transport and augmented radiation sensitivity caused by loss of RLIP76. FEBS Lett. 2008; 582:3408–14. [PubMed: 18789326]
30. Singhal SS, Wickramarachchi D, Singhal J, Yadav S, Awasthi YC, Awasthi S. Determinants of differential doxorubicin sensitivity between SCLC and NSCLC. FEBS Lett. 2006; 580:2258–64. [PubMed: 16579994]
31. Singhal SS, Awasthi YC, Awasthi S. Regression of melanoma in a murine model by RLIP76-depletion. Cancer Res. 2006; 66:2354–60. [PubMed: 16489041]
32. Singhal SS, Singhal J, Yadav S, et al. Regression of lung and colon cancer xenografts by depleting or inhibiting RLIP76. Cancer Res. 2007; 67:4382–9. [PubMed: 17483352]
33. Singhal SS, Singhal J, Yadav S, Sahu M, Awasthi YC, Awasthi S. RLIP76: A target for kidney cancer therapy. Cancer Res. 2009; 69:4244–51. [PubMed: 19417134]
34. Singhal SS, Roth C, Leake K, Singhal J, Yadav S, Awasthi S. Regression of prostate cancer xenografts by RLIP76 depletion. Biochem Pharmacol. 2009; 77:1074–83. [PubMed: 19073149]
35. Singhal SS, Sehrawat A, Sahu M, et al. RLIP76 transports sunitinib and sorafenib and mediates drug resistance in kidney cancer. Int J Cancer. 2010; 126:1327–38. [PubMed: 19626587]
36. Chan KS, Sano S, Kiguchi K, et al. Disruption of Stat3 reveals a critical role in both the initiation and the promotion stages of epithelial carcinogenesis. J Clin Invest. 2004; 114:720–8. [PubMed: 15343391]
37. Chan KS, Sano S, Kataoka K, et al. Forced expression of a constitutively active form of Stat3 in mouse epidermis enhances malignant progression of skin tumors induced by two-stage carcinogenesis. Oncogene. 2008; 27:1087–94. [PubMed: 17700521]
38. Rosse C, L'Hoste S, Offner N, Picard A, Camonis JH. RLIP76, an effector of the Ral-GTPases, is a platform for Cdk1 to phosphorylate epsin during the switch off of endocytosis in mitosis. J Biol Chem. 2003; 278:30597–604. [PubMed: 12775724]
39. Kariya K, Koyama S, Nakashima S, Oshiro T, Morinaka K, Kikuchi A. Regulation of complex formation of POB1/epsin/adaptor protein complex 2 by mitotic phosphorylation. J Biol Chem. 2000; 275:18399–406. [PubMed: 10764745]
40. Hitchens TK, Mannervik B, Rule GS. Disorder-to-order transition of the active site of human class Pi glutathione transferase, GST P1–1. Biochemistry. 2001; 40:11660–9. [PubMed: 11570866]
41. Chuang CC, Wu SH, Chiou SH, Chang GG. Homology modeling of cephalopod lens S-crystallin: a natural mutant of sigma-class glutathione transferase with diminished endogenous activity. Biophys J. 1999; 76:679–90. [PubMed: 9929473]
42. Tomarev SI, Zinovieva RD, Guo K, Piatigorsky J. Squid glutathione S-transferase. Relationships with other glutathione S-transferases and S-crystallins of cephalopods. J Biol Chem. 1993; 268:4534–42. [PubMed: 8440736]
43. Awasthi S, Cheng J, Singhal SS, et al. Functional reassembly of xenobiotic transport from the N-terminal and C-terminal domains of RLIP76 and identification of ATP binding sequences. Biochemistry. 2001; 40:4159–68. [PubMed: 11300797]
44. Awasthi S, Bajpai KK, Singhal SS, Frenkel EP, Ansari GAS, Awasthi YC. The effect of glutathione S-transferases on interactions of glutathione and melphalan. Drug Metab Disp. 1996; 24:371–4.
45. Singhal SS, Yadav S, Singhal J, Drake K, Awasthi YC, Awasthi S. The Role of PKCα and RLIP76 in Transport-mediated Doxorubicin-resistance in Lung Cancer. FEBS Lett. 2005; 579:4635–41. [PubMed: 16087181]
46. Singhal SS, Yadav S, Singhal J, et al. Depletion of RLIP76 sensitizes lung cancer cells to doxorubicin. Biochem Pharmacol. 2005; 70:481–8. [PubMed: 15950949]
47. Sharma R, Haque AK, Awasthi S, Singh SV, Piper JT, Awasthi YC. Differential carcinogenicity of benzo(a) pyrene in male and female CD-1 mouse lung. J Toxicol Environ Health. 1997; 52:45–62. [PubMed: 9269322]
48. Awasthi S, Singhal SS, Yadav S, et al. A central role of RLIP76 in regulation of glycemic control. Diabetes. 2010; 59:714–25. [PubMed: 20007934]

49. Cheng JZ, Sharma R, Yang Y, et al. Accelerated metabolism and exclusion of 4-hydroxynonenal through induction of RLIP76 and hGST5.8 is an early adaptive response of cells to heat and oxidative stress. J Biol Chem. 2001; 276:41213–23. [PubMed: 11522795]

50. Michie AM, Nakagawa R. The link between PKCα regulation and cellular transformation. Immunol Lett. 2005; 96:155–62. [PubMed: 15585319]

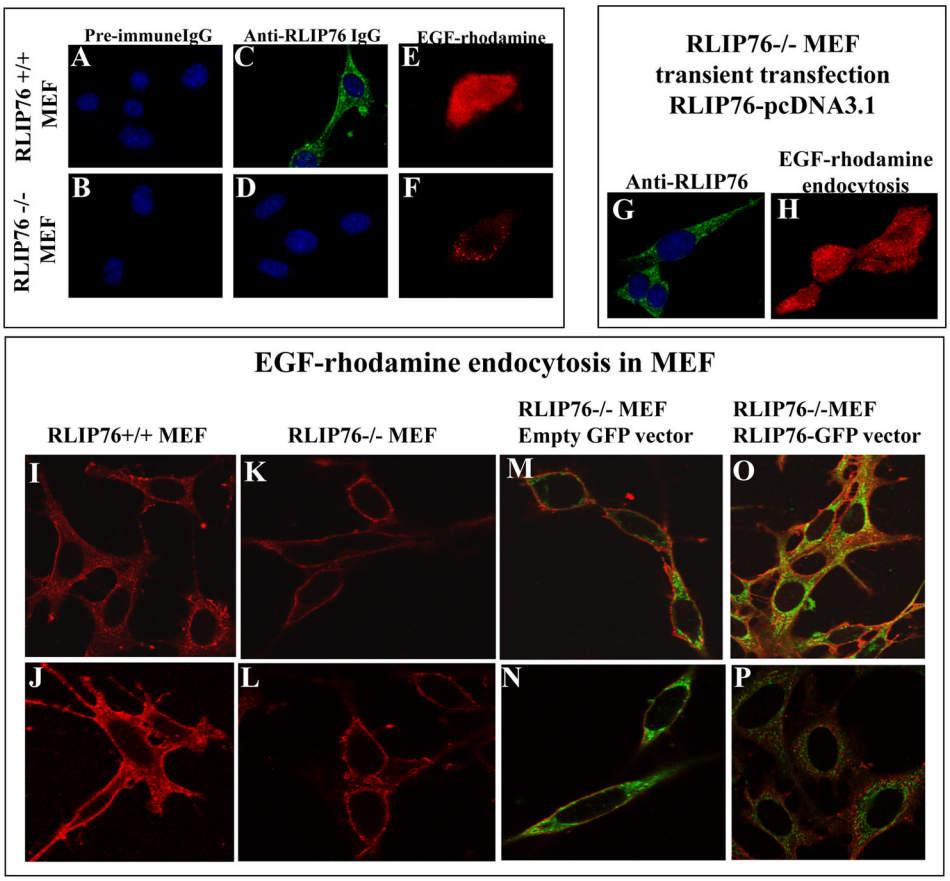

Figure 1. EGF-rhodamine endocytosis is deficient in RLIP76$^{-/-}$ MEFs, and is restored completely by transient transfection with wild-type RLIP76

RLIP76$^{-/-}$ MEFs were treated with pre-immune IgG (**A and B**), anti-RLIP76 IgG (**C and D**) and EGF-rhodamine endocytosis (at 10 min) (**E and F**). Nuclei are stained with DAPI (**panel A-F**). Transfection of RLIP76 restores IHC-detectable RLIP76 in the RLIP76$^{-/-}$ cells (**panel G**), and EGF-rhodamine endocytosis is fully restored (**panel H**). GFP-RLIP76 construct in pcDNA3.1 was used to transfect RLIP76$^{-/-}$ MEFs to show that the entry of EGF-rhodamine into the cells is deficient in RLIP76$^{-/-}$, that empty-vector GFP does not restore this, and that its entry into RLIP76$^{-/-}$ cells is restored by transfection with GFP-RLIP76 (two representative micrographs are presented for each of four experimental groups) (**panels I-P**). Quant Image-J software was used for image analyzing and quantifying fluorescence per area by blinded observers. Photographs were taken at identical exposures using 400 × magnifications.

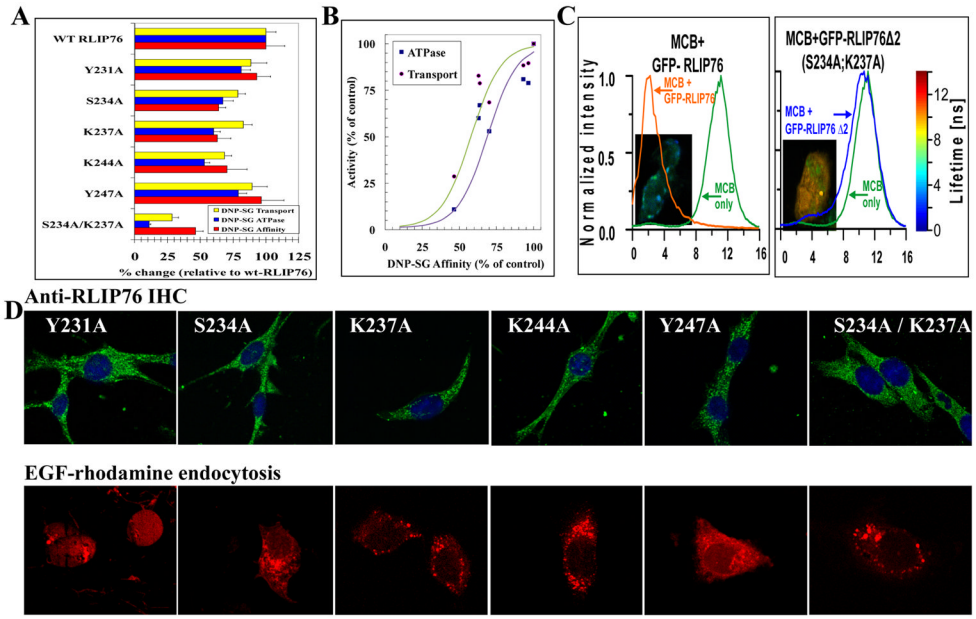

Figure 2. Effect of mutations on GS-E affinity, ATPase activity

Equal amounts of the purified protein (15 μg) was added to DNPSG-Sepharose-4B affinity-resin for 1h, and un-bound RLIP76 was measured in the supernatant by ELISA assay (standard curve r2 0.99) and 1/unbound was used as for DNPSG-affinity. DNPSG-stimulated ATPase-activity of each mutant was measured as previously described (19). The ATP-dependent DNP-SG transport-activity was determined after reconstituting the purified recombinant proteins into artificial asolectin-cholesterol liposomes as described previously (19). All results were normalized to control, wild-type RLIP76. Percent residual-activity is shown (**panel A**). A plot of DNPSG-affinity vs. either ATPase or transport-activity normalized to wild-type is presented (**panel B**). The effect of these mutations on GS-E binding was studied using the GSH-monochlorobimane (GSH-MCB) fluorescent-conjugate. RLIP76 MEF$^{-/-}$ cells transfected with RLIP76-GFP vector were treated with 50 μM monochlorobimane (which gives rise to a fluorescent GSH-conjugate in cells) for 20 min at 37°C prior to 4 % paraformaldehyde fixation, followed by molecular interaction analysis using FRET using time-resolved confocal microscope MT 200 (from Picoquant GmbH) with pulsed diode laser excitations at 405 nm (for MCB donor) and 475 nm (for GFP donor). For MCB observation, 465 nm (10 nm band width) interference filter crossed with 430 nm long path cut-off and for GFP observation 490–530 nm interference filter crossed with 500 nm long path filter was used. The histogram graph presents observed fluorescence lifetime measured for the respective images, MCB alone (green) RLIP76-GFP (red) (**panel C, left**). There is no significant change in the fluorescence life time cells transfected with the mutant of RLIP76 lacking GSH-binding site (ΔS234A/K237A) (blue) (**panel C, right**). The mutant RLIP76 cDNAs were cloned into pcDNA3.1 eukaryotic expression vector, and successful transient transfection of RLIP76$^{-/-}$ MEFs was demonstrated by IHC against RLIP76 with FITC-labeled secondary antibody **(panel D, top row)**, and representative photomicrographs of RLIP76-mutant transfected cells showing the consequent partial restoration of EGF-rhodamine endocytosis are shown **(panel D, bottom row)**.

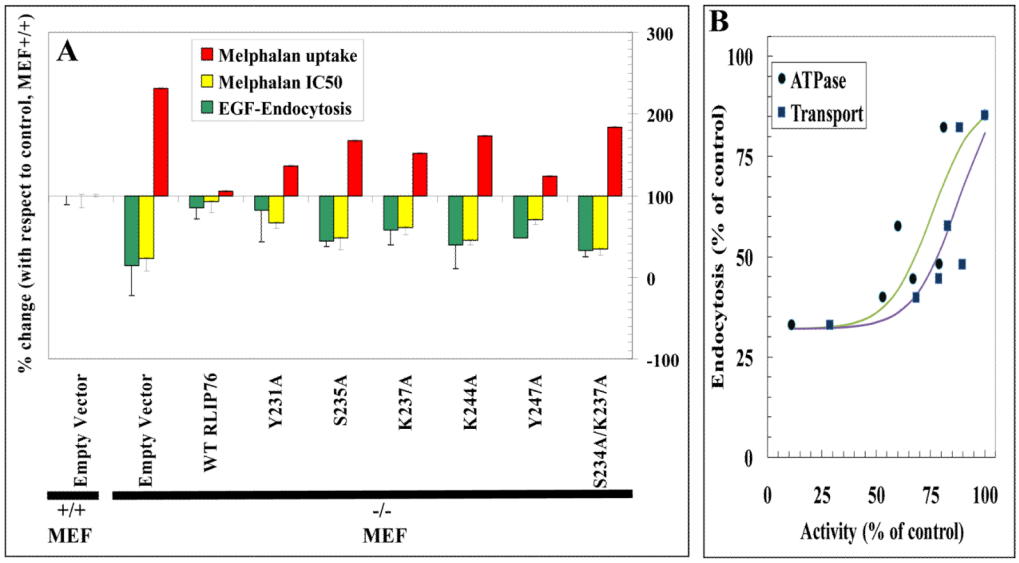

Figure 3. Functional-activity of RLIP76 mutants in MEFs

The IC50 of the glutathione-conjugate metabolized drug melphalan was determined for each cell line by MTT assay, the cellular accumulation of ^{14}C-melphalan at 30 min after exposure was determined as described previously (20,22), and results of separate studies of endocytosis quantified by Image-J software are presented. All studies were done three times with triplicate determinations each time (**panel A**). A plot showing endocytosis activity of each mutant plotted against either the ATPase-activity (**round symbols**) or transport-activity (**square symbols**) is shown with a logistical regression curve demonstrating a direct and saturable relationship of CDE with these measures of activity (**panel B**).

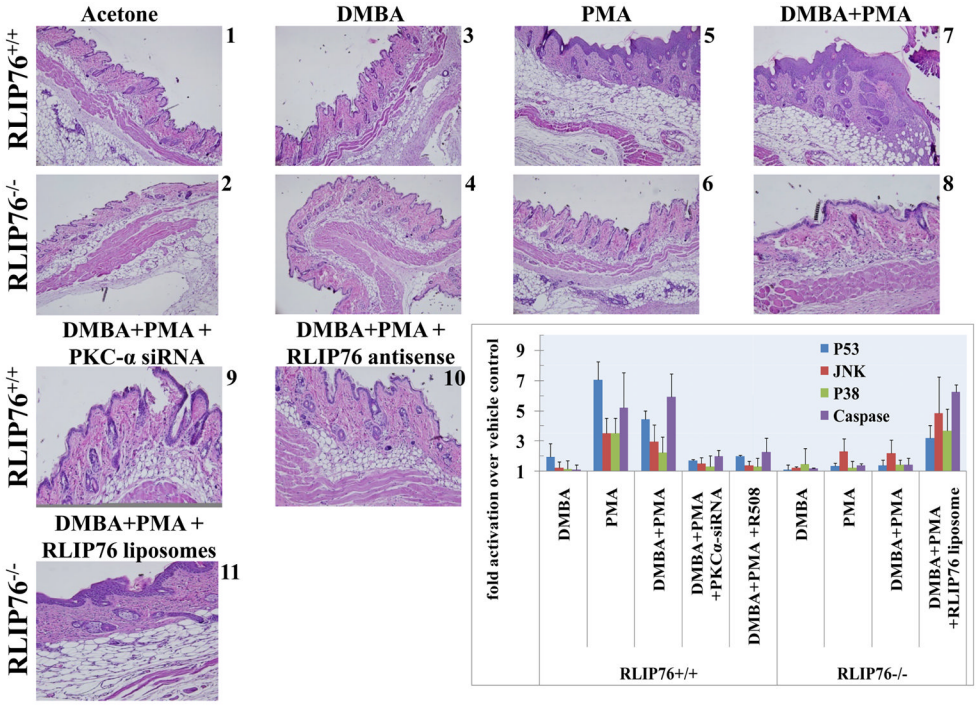

Figure 4. RLIP76 and PKCα are both necessary for DMBA/PMA skin-carcinogenesis

The experiment was carried out in wild-type (RLIP76$^{+/+}$) and RLIP76 knockout (RLIP76$^{-/-}$) C57B male mice. The skin of the back was shaved and 25 nmol DMBA or vehicle control (acetone) was applied to a 1 cm^2 patch of shaved skin (36,37). After two weeks, on day 14, RLIP76$^{+/+}$ animals were injected *i.p.* with 200 μL PBS with or without either PKCα-siRNA or RLIP76-antisense (R508). Also on day 14, RLIP76-liposomes were applied to the skin of one group of RLIP76$^{-/-}$ mice. On day 15, 10 nmol PMA in acetone or acetone alone were applied to the skin. The animals were sacrificed 4 days later and skin was harvested for histological and biochemical analyses. Animals in 11 treatment groups were treated as indicated in the figure. Levels of phosphorylated JNK, p38, p53 (Active-Motif) and total caspase (Immunochemistry Technologies) were determined using ELISA assays, and normalized to the values found in vehicle-control skin. Values presented are mean and s.d. of three determinations of fold-activation from n = 8 animals per group.

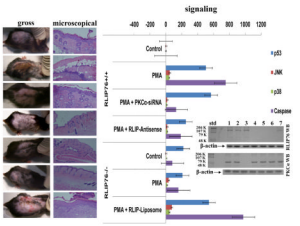

Figure 5. RLIP76 and PKCα are both necessary for chloroform/PMA skin-carcinogenesis

The experiment was carried out in RLIP76$^{+/+}$ and RLIP76$^{-/-}$ C57B male mice. On day 1, RLIP76$^{+/+}$ animals were injected *i.p.* with 200 μL PBS with or without either PKCα-siRNA, or RLIP76-antisense (R508). Also on day 1, RLIP76-liposomes were applied to the skin of one group of RLIP76$^{-/-}$ mice. On day 2, 10 nmol PMA in chloroform or chloroform alone were applied to the skin. The animals were sacrificed on day 6 and skin was harvested for histological and biochemical analyses. Photographs of representative animals from each group and H&E stained histological sections as well as levels of phosphorylated JNK, p38, p53 (Active-Motif) and total caspase (Immunochemistry Technologies) are presented. Skin from three animals from each of 7 groups was analyzed for p53, JNK, p38, and total caspases. Values presented are mean and s.d. of triplicate determinations of fold-activation with respect to the vehicle-control group. RLIP76 and PKCα protein in 28,000 × g supernatants of skin homogenate was determined by Western-blot analyses using anti-RLIP76, and anti-PKCα antibodies **(inset)**.

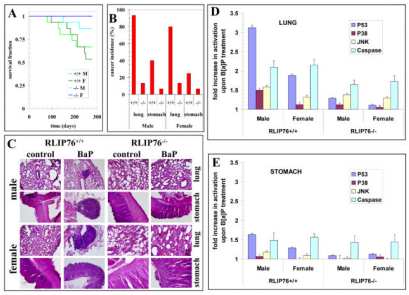

Figure 6. Absence of RLIP76 reduces B[a]P-mediated lung and stomach adenocarcinomas

These experiments 15 animals per group, twelve-weeks-old, 30 male and 30 female each RLIP76$^{+/+}$ and RLIP76$^{-/-}$ mice, divided into two groups (control and BaP treatment). Animals were treated with 3 mg BaP in 0.2 mL corn oil, twice 4-weeks apart, or an equal volume of corn oil. Surviving animals were sacrificed at 9 months by CO2 inhalation followed by cervical dislocation after ~36 weeks from the beginning of the experiment and the lungs and stomach were harvested for histopathological examination. Percent surviving in each group **(panel A)**, cancer incidence determined by complete autopsy **(panel B)** and representative photomicrographs of H stained histological slides **(panel C)** are presented. Fold change in p53, p38, JNK and caspase-activation in lung **(panel D)** and stomach **(panel E)** tissues of male and female RLIP76$^{+/+}$ and RLIP76$^{-/-}$ as compared with respective vehicle control treated group are presented for n = 3 animals per group. The numbers of carcinomas in different groups were compared by ANOVA.